High fidelity model of pipe bundle coupling mechanism in nuclear fusion plant remote maintenance

Proceedings of the ASME 2024
International Mechanical Engineering Congress and Exposition
IMECE2024
November 17-21, 2024, Portland, Oregon

IMECE2024-145583

HIGH FIDELITY MODEL OF PIPE BUNDLE COUPLING MECHANISM IN NUCLEAR FUSION PLANT REMOTE MAINTENANCE

Mario Troise
Politecnico di Torino
Turin, Italy

Martina Ferrauto
Politecnico di Torino
Turin, Italy

Matteo Gaidano
Politecnico di Torino
Turin, Italy

Matteo Melchiorre
Politecnico di Torino
Turin, Italy

Davide Sorli
Politecnico di Torino
Turin, Italy

Stefano Mauro
Politecnico di Torino
Turin, Italy

ABSTRACT

Periodically maintenance of Plasma-Facing Components (PFCs) are one of the critical issues in DEMOnstration (DEMO) reactor. The harsh environment of a fusion reactor dictates remote maintenance, which requires the development of new strategies and technologies. Indeed, a Service Joining System (SJS) for in-bore cutting and welding has been designed for PFC replacements. Therefore, strict alignment requirements between welding surfaces must be ensured. The alignment task involves a first phase of positioning during which the new pipes are brought close to their final position, and in the second phase a robot system ensures precise pipe coupling.

This paper presents the high-fidelity model of the Laser Bore Joint (LBJ), focusing on the pipe bundle coupling mechanism. The flexible elements of the LBJ have been described using both analytical and Finite Element Analysis (FEA). The bellow stress-strain diagram has been obtained, which shows the effect of its anelasticity when the alignment force increases. Furthermore, the Lumped Parameter Model (LPM) of the bellow and their use in the LBJ multibody model are presented. Finally, the contact parameters and two different cuff designs of the LBJ are analyzed. The simulation results are shown and discussed.

Keywords: DEMO, Multibody, Alignment, Bellow, Lumped Parameters, Remote Maintenance

1. INTRODUCTION

In the last decades, the European fusion program has conducted several conceptual design studies that aim to produce electricity by nuclear fusion around the middle of this century [1, 2]. In this context, the DEMO fusion reactor serves as the initial prototype for a nuclear fusion facility. DEMO will operate using a closed fuel cycle and aims to generate 300-500 megawatts (MW) of electrical energy for the grid. The Nuclear Power Plant (NPP) design process began in 2014 and is currently in the pre-conceptual design stage. Various development teams can propose different design solutions to enhance safety, operational reliability, availability, and reduce maintenance costs for the DEMO reactor [3].

The development of a maintenance strategy to replace DEMO in-vessel components after completion of their lifecycle or in case of failure is one of the critical issues to the successful development of fusion energy. However, due to neutron activation, manual maintenance is precluded within the bio-shield and in many areas of the plant. Therefore, Remote Maintenance (RM) is needed [4]. Furthermore, The remote maintenance project must provide the limits of the strategy and technologies to modify correctly the plant design [5], and its must also comply with the nuclear regulations and safety standards [6].

The engineering and the periodically replacement of the PFCs covering the plasma chamber wall, which must operate reliably in an extreme environment are critical challenges. PFCs include the blanket modules that absorb the fusion energy, and the divertor that exhausts the plasma impurities and heat [7]. Furthermore, PFCs must be designed to minimize the tritium release and, to facilitate the remote handling and inspection [8]. The overall requirements, methods developed for PFCs assessment, and the status of the designs are discussed in [9].

Demo Tokamak will have three types of maintenance ports: upper, lower, and equatorial [10]. Maintenance ports will be used

for maintaining and replacing components within the tokamak structure [5]. Within upper and lower ports, the Pipe Modules (PMs) of the blanket will be replaced using a SJS with LBJ for in-situ cutting and welding [11]. LBJ involves a set of pins and holes intended to drive the operation, together with flexible bellows, that give compliance both in axial and radial directions [12]. A failure in the alignment phase would make welding impossible [13]. The alignment task starts moving the new pipes near their final position by a primary system, following a robotic system with suitable a vision sensor [14], that ensures the fine positioning of the pipes [15].

Thermal expansion is a critical issue in NPP piping and the use of bellows increases the flexibility of the pipes [16]. Bellows are convoluted shells connected with annular plates [17] and they are largely used in sea environments [18]. Bellows provide additional flexibility in piping and heat exchanger shell, they must withstand their internal fluid pressure while absorbing axial, bending deflections, and lateral displacement. Their use in NPP is described in [19, 20] and the bellows failure mode is discussed in [21]. Furthermore, a digital twin, as presented in [22], can be designed for the bellow and SJS to investigate how the failure of the bellows affects the system. Accurate analysis of multilayer bellows requires numerical methods beyond linear thin shell theory, these methods consider complex layer interactions. Simplified design criteria are commonly employed alongside elastic analysis, even for nonlinear and high-temperature failure modes. In this context, Anderson theory [23, 24] can be applied to multilayer bellows to calculate their stiffness. Furthermore, numerical and theoretical methods are used to predict the bellows response [25] and a pseudo-rigid body approach, as [26, 27], can be applied to model them.

This work presents the high-fidelity model of the Laser Bore Joint , focusing on the piping coupling. The secondary handling strategy and the sensor layout have been presented in previous work [28]. Bellows stiffness using both analytical and finite element analysis has been calculated and their values are compared. The stress-strain diagram of the bellow is presented showing their plastic behaviour under high forces. Furthermore, the lumped parameter model of the bellow and two different cuffs designs are proposed. Finally, the simulation results are shown and discussed.

2. LASER BORE JOINT

The LBJ leads a main role in the operation of SJS, providing several functions such as weld preparation protection, pipe alignment, the provision of backing gas, and debris capture [12]. **FIGURE 1** shows the LBJ concept system, which has one bellow of 80 mm diameter (DN80) and two bellows of 200 mm diameter (DN200).

In the First Wall, there are the most critical connections, requiring high integrity to protect the vacuum in the tokamak needed for operation, especially challenging if helium is used as a coolant. The pulsed operation of DEMO applies cycling thermal stress on the first wall components, then a periodically replaced mu be considered. The current configuration of DEMO relies on clustering several pipes in a small area to provide the necessary services to the First Wall components [12], the piping will be replaced using SJS and LBJ. After removing the worn pipes, the new pipes must be inserted and aligned correctly. In the first alignment phase the pins, holes, and cuffs guide the cuff surfaces near. The cuff design must ensure tight tolerances and provide an enclosure for SJS cutting and welding operations. The compliance is provided by flexible bellows and constraining rings. The alignment terminates with contact between bump stops.

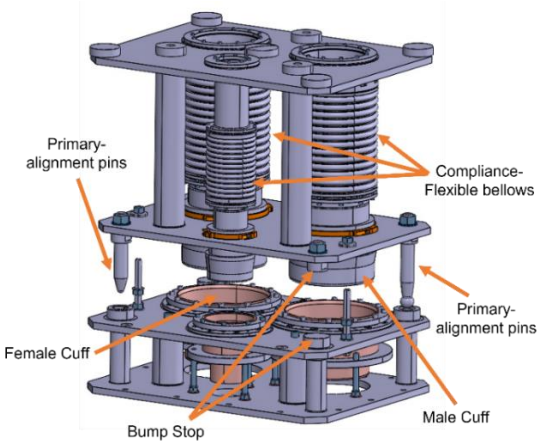

FIGURE 1: LBJ CONCEPT DESIGN

The LBJ alignment task will be performed using both the upper and lower maintenance ports. A crane will be the Primary Handling System (PHS) for the upper port, and a dexterous arm with a 500 kg payload will be the Secondary Handling System (SHS).

3. BELLOW MODEL

Bellows on both ends of the LBJ compensate for small misalignments and small deviations in nominal length and allow compression for flange separation when removing a module [29]. Bellows are made of Inconel 625 strengthened by the addition of carbon, chromium, molybdenum, and niobium. They are characterized by excellent static, fatigue, and creep resistance, with operating temperatures ranging from -196°C to 982°C. Additionally, they exhibit outstanding resistance to pitting and crevice corrosion. The bellows material has a density of $\rho = 8.44$ g/cm³, a maximum yield strength of 1013 MPa, and a Young's modulus E = 205 GPa, at a temperature of 20°C, with a Poisson's ratio of 0.3 [30]. **FIGURE 2** shows the typical bellows layers.

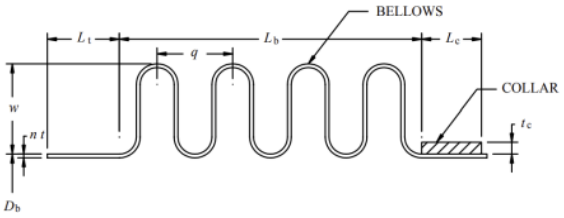

FIGURE 2: BELLOWS GEOMETRY PARAMETERS

The main parameters of bellows layers are: number of convolutions, n_w, number of layers, n, thickness of a single layer, t, tangent collar thickness, t_c, bellows length, L_b, bellows height, w, base diameter, D_b, convolution spacing, q, average diameter, D_m. In the currently design the bellows have two size:

a) **DN200**: Diameter 265 mm, 25 kg weight, 314 mm length, 7 layers with 0,7 mm thickness.
b) **DN100**: Diameter 149 mm, 5 kg weight, 208 mm length, 7 layers with 0,5 mm thickness.

The bellow DN200 is shown in **FIGURE 3**, and the parameters of the bellows DN200 and DN100 are reported in **TABLE 1.**

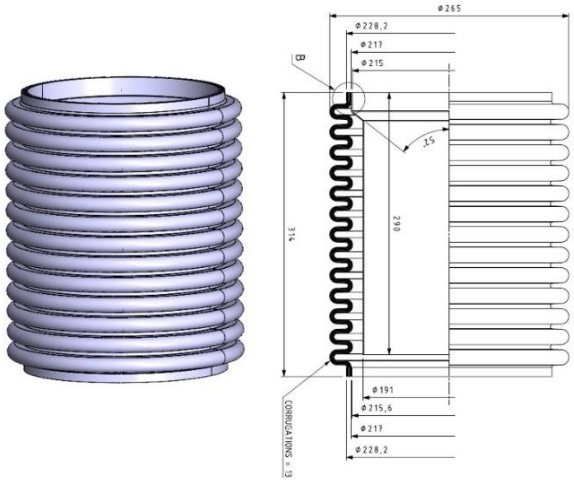

FIGURE 3: CROSS-SECTION OF THE BELLOW DN200

TABLE 1: GEOMETRIC PARAMETERS OF THE BELLOWS

Parameter	DN200	DN100
$L_b\ [mm]$	294	180
$D_m\ [mm]$	238.3	136.5
$w\ [mm]$	18.4	13
$t_c\ [mm]$	1.0	1.0
$t\ [mm]$	0.7	0.5
$n_w\ [-]$	13	12
$n\ [-]$	7	7
$D_b[mm]$	215	120
$q\ [mm]$	22.62	15.00
$t_p\ [mm]$	0.665	0.470

The bellows axial stiffness has been calculated using EJMA standards [31]:

$$c_{ax} = 1{,}7\frac{D_m\ E\ t_p^3\ n}{w^3\ C_f\ n_w} \tag{1}$$

Where C_f is a dimensionless coefficient dependent on the geometry of the bellows, determined from the graph in [31]. Additionally, the bellow stiffnesses have been calculated using the Witzenmann manual to compare the results with EJMA. The stiffnesses formulation according to Witzenmann are reported below:

$$c_{ax} = \frac{E}{2(1-\nu^2)}\frac{\pi D_m\ t^3}{w^3}\frac{n}{n_w}\frac{1}{C_f} \tag{2}$$

$$c_{lat} = \frac{3}{2}\frac{D_m}{L_b}\ c_{ax} \tag{3}$$

$$c_{ang} = \frac{D_m^2}{8}\ c_{ax} \tag{4}$$

Where c_{ax} is the bellow axial stiffness, c_{lat} is the lateral stiffness, and c_{ang} is the angular stiffness. In **TABLE 2** and **TABLE 3** the bellows stiffness of DN200 and DN100 according to EJMA and Witzenmann are compared.

TABLE 2: DN200 STIFFNESS VALUES

Stiffness	EJMA	Witzenmann	Difference [%]
c_{ax}	$1114.9\ \left[\frac{N}{mm}\right]$	$1136.6\ \left[\frac{N}{mm}\right]$	-1.95
c_{lat}	$1355.5\ \left[\frac{N}{mm}\right]$	$1381.9\ \left[\frac{N}{mm}\right]$	-1.95
c_{ang}	$7913.9\ \left[\frac{Nm}{\deg}\right]$	$8067.9\ \left[\frac{Nm}{\deg}\right]$	-1.95

TABLE 3: DN100 STIFFNESS VALUE

Stiffness	EJMA	Witzenmann	Difference [%]
c_{ax}	$1096.3\ \left[\frac{N}{mm}\right]$	$1210.8\ \left[\frac{N}{mm}\right]$	-10.44
c_{lat}	$1247.1\ \left[\frac{N}{mm}\right]$	$1377.3\ \left[\frac{N}{mm}\right]$	-10.44
c_{ang}	$2553.4\ \left[\frac{Nm}{\deg}\right]$	$2820.2\ \left[\frac{Nm}{\deg}\right]$	-10.45

Comparing the stiffness values according to EJMA with Witzenmann's formulation, the difference is less than 2% for the bellow DN200 and 10% for bellow DN100. Subsequently, the axial stiffness values have been verified through finite element analysis using Partial Differential Equation toolbox of Matlab. Due to the high geometric complexity of the bellows, which increases the computational load, finite element analysis is conducted on bellows with a single layer and an equivalent thickness ensuring the same axial stiffness. The equivalent thickness has been calculated using Anderson's theory [23, 24], then the axial stiffness has been evaluated according EJMA and Witzenmann manual. Results obtained using both methods are consistent, the equivalent thicknesses for DN100 and DN200 are reported in **TABLE 4**.

TABLE 4: EQUIVALENT THICKNESSES

Equivalent thicknesses	EJMA Standard [mm]	Witzenmann [mm]
DN200	1.272	1.272
DN100	0.897	0.897

The FEA axial displacement using bellows with equivalent thickness are shown in **FIGURE 4** and **FIGURE 5**.

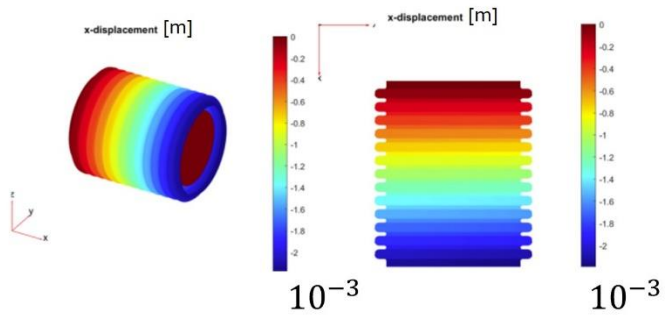

FIGURE 4: DN200 FEA ANALYSIS WITH $F = 2400$ N

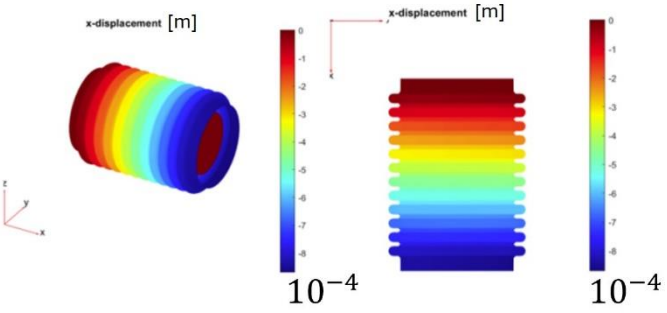

FIGURE 5: DN100 FEA ANALYSIS WITH $F = 1200$ N

The axial stiffness results from Matlab FEA is 1151.5 N/mm for DN200 and 1213.5 N/mm for DN100. Furthermore, ANSYS software to describe the non-linear behaviour of the bellows as a function of axial applied force has been used. The stress-strain diagram of the bellow DN200 with equivalent thickness has been reported in **FIGURE 6** TET10 elements with 0.005 m size have been used for ANSYS mesh. The axial stress-strain curve has been compared to theoretical elastic behaviour using Witzenmann stiffness to underline the plastic deformation.

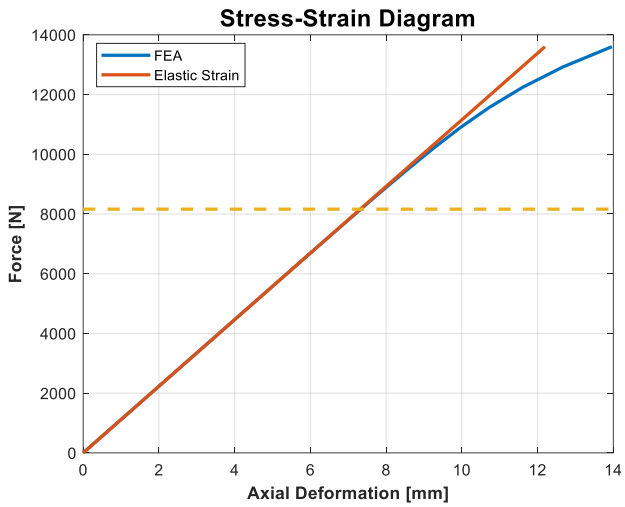

FIGURE 6: PLASTIC BEHAVIOUR OF BELLOW DN200 WITH ANSYS FEA

The elastic axial stiffness of DN200 obtained from ANSYS FEA is 1135.5 N/mm. Finally, in **TABLE 5** the elastic axial stiffness of DN200 calculated with EJMA, Witzenmann, Matlab FEA, and ANSYS FEA are compared. Results from different approaches are consistent and the bellows stiffnesses have been used in the lumped parameter model described in the next paragraph.

TABLE 5: ELASTIC AXIAL STIFFNESS OF DN200

Method	Axial Stiffness $\left[\frac{N}{mm}\right]$
EJMA	1114.9
Witzenmann	1136.6
Matlab FEA	1151.5
ANSYS FEA	1135.5

4. LUMPED PARAMETER MODEL OF THE BELLOWS

A multibody model of the LBJ in an Adams environment to analyze primary alignment dynamics has been developed. Bellows have been modeled using a lumped parameter model, to reduce computational load without compromising the accuracy of dynamic analyses. The LPM is a multi-degree of freedom (MDOF), consisting of masses interconnected through axial, lateral, and torsional dampers and stiffnesses. The mass, stiffness, and damper values have been determined to preserve

the static and dynamic response of the bellows, ensuring good quality in the simulations for the alignment of the LBJ. Finally, the axial, lateral, and torsional natural frequencies of the bellows are analytically determined, approximating it as a fixed-free Euler-Bernoulli beam, and then verified against those obtained through FEA analysis. The natural frequencies of DN200 as a function of the i-th mode of vibration are reported in **FIGURE 7**, **FIGURE 8** and **FIGURE 9**.

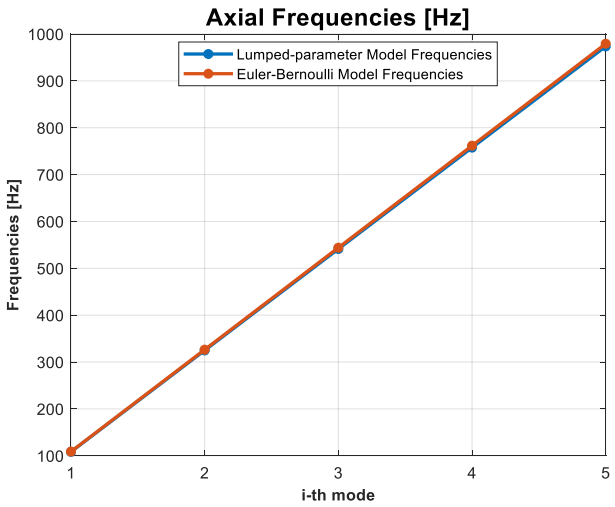

FIGURE 7: AXIAL FREQUENCIES OF BELLOWS DN200

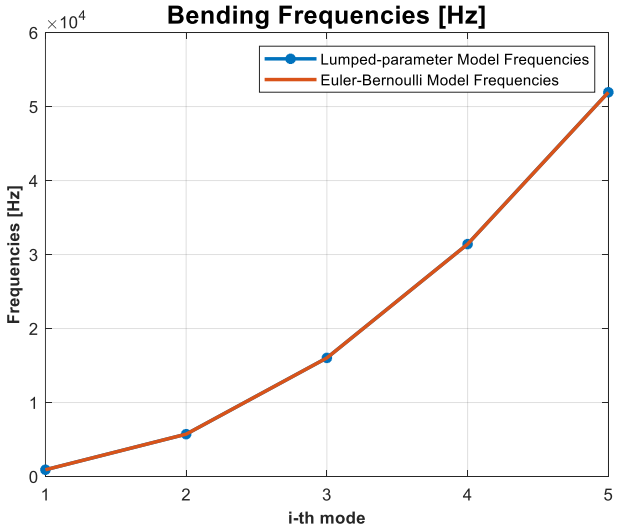

FIGURE 8: BENDING FREQUENCIES OF BELLOWS DN200

The axial and bending natural frequencies with Euler-Bernoulli and LPM present a minimal absolute difference across all relevant frequencies. However, when i-th frequency increases, the difference increases, particularly on torsional frequencies. This result can be attributed to the specific geometric characteristics of the bellow. Accurate torsional frequency description requires adaptation of the Euler-Bernoulli theory, nevertheless, the torsional dynamic is not relevant in the LBJ alignment and the presented LPM can be applied.

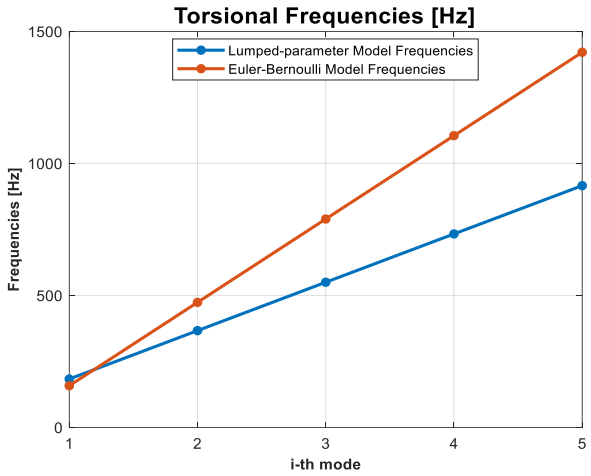

FIGURE 9: TORSIONAL FREQUENCIES OF BELLOWS DN200

Results obtained from DN100 are comparable to DN200, confirming the LPM validity. Finally, an analysis varying the DOF, from 10 to 100, of the LPM is presented in **FIGURE 10**.

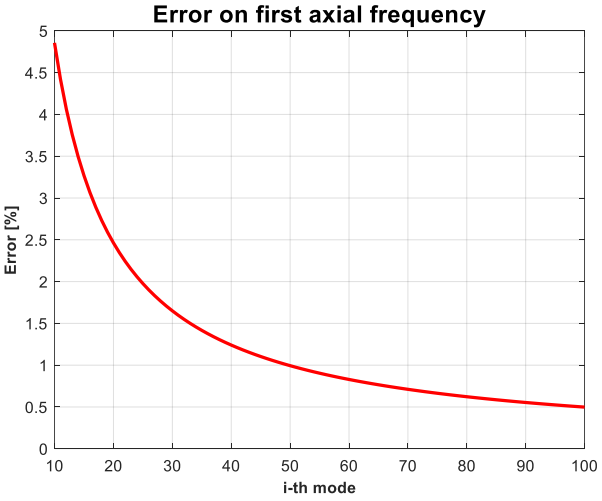

FIGURE 10: ERROR ON FIRST AXIAL FREQUENCY BETWEEN EULER-BERNOULLI BEAM THEORY AND LPM

Increasing the number of masses progressively reduces the error on the first axial frequency. This enables a more accurate description of local stiffness and mass distribution along the bellows' length, impacting natural frequencies and dynamic responses. Nevertheless, even with 10 DOF, the analysis yields a good natural frequency description, with an error below 5%. Therefore the LBJ multibody analyses have been conducted using bellows LPM with 10 DOF to reduce simulation load and time.

5. MULTIBODY MODEL

The multibody model of the LBJ, shown in **FIGURE 11**, has been developed in ADAMS environment using the LPM of the bellows with 10 DOF due to load computation of flexible bodies [32]. The model includes all the important parts of the assembly: cuffs, bellows, and a rigid structure that drives the movement of the pipes module, their inertial properties, the kinematic constraints, and the interaction forces. The parts that are not relevant to the pipe bundle coupling and do not affect the system dynamic have been excluded.

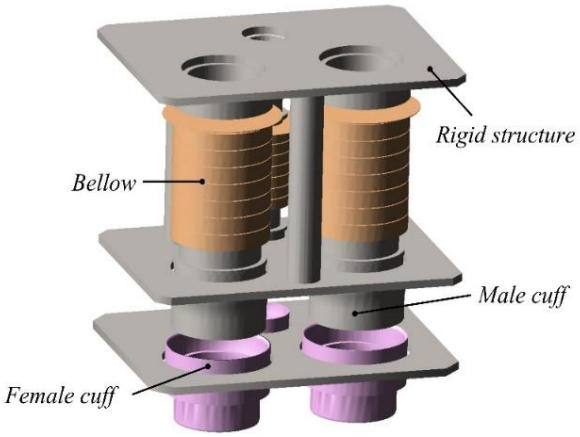

Figure 11: MULTIBODY MODEL OF LBJ IN ADAMS

The first and the last masses of the bellows LPM have been rigidly constrained to the rigid structure and male cuffs. Instead, bushing elements between the internal masses of the bellow have been used to allow relative displacements and rotations, as shown in **FIGURE 12**. The bushing joint is characterized by both stiffness and linear damping, it connects two bodies providing both force and torque reactions allowing deformations and rotations description between cuffs during alignment.

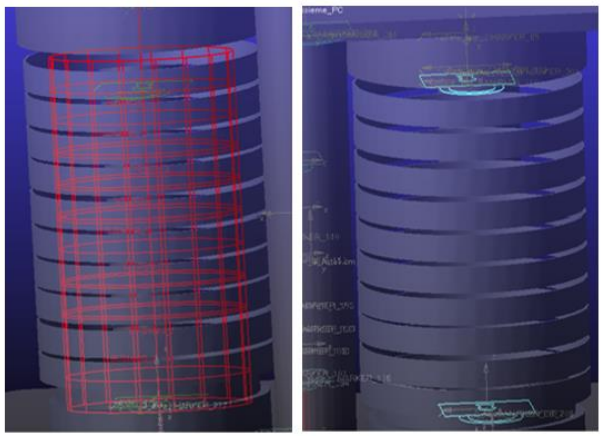

FIGURE 12: BUSHING ELEMENTS AND FIXED JOINTS

5.1 Contact Model Parameters

The contact forces can be described using a three-dimensional multibody model [33], lumped parameters modelling [34] or high-fidelity model, as [35]. To describe the contact forces between cuffs the equation below has been used:

$$F = k(q_0 - q)^e - c_{\mathrm{m}}\dot{q} \cdot STEP(q, q_0 - d, 1, q_0, 0) \qquad (8)$$

where q_0 is the trigger distance at which the contact begins, q is the penetration depth, $STEP$ is the damping ramp-up exponential function, e is the force exponent, k is the contact stiffness, c_{m} is the maximum contact damping value and d is the penetration depth at which the contact damping is maximum. The contact stiffness and the damping value depend on the material properties and contact geometry. Recommended values are discussed in [36], nevertheless, appropriate values for each parameter must be determined through an iterative process or experimental tests. In this work, the contact model parameters have been determined imposing an axial and radial misalignment between male and female cuffs into the multibody model, results are discussed below.

Initially, the contact stiffness value has been modified between 10^7 and $10^{11}\ N/m$. Indeed, below $10^7\ N/m$ an excessive penetration occurs between cuffs that do not allow a fidelity contact description. On the other hand, for higher values of contact stiffness, the system response becomes inconsistent and lacks physical sense, as shown in **FIGURE 16**. The cuffs misalignment and system response have been studied by varying the contact stiffness, results are reported in **FIGURE 13, FIGURE 14**, **FIGURE 15** and **FIGURE 16.**

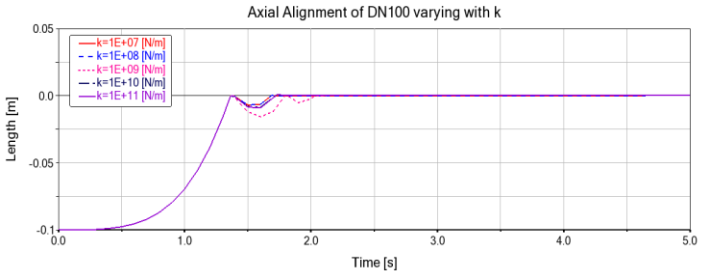

FIGURE 13: AXIAL ALIGNMENT OF DN100

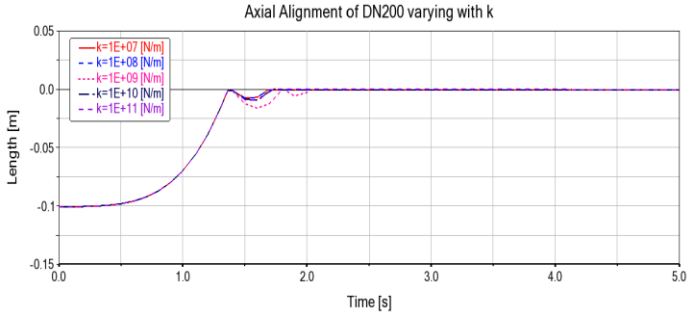

FIGURE 14: AXIAL ALIGNMENT OF DN200

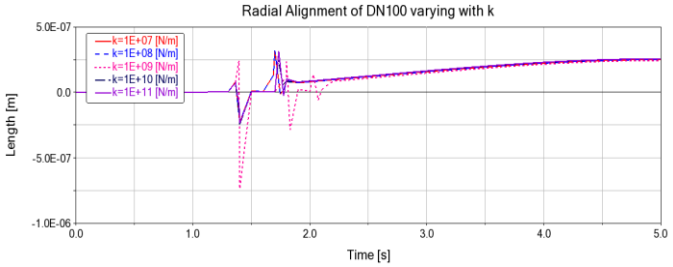

FIGURE 15: RADIAL ALIGNMENT OF DN100

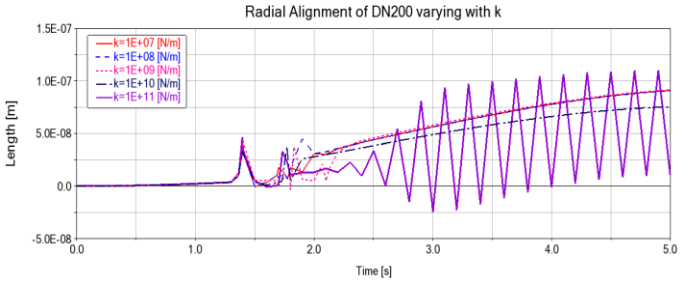

FIGURE 16: RADIAL ALIGNMENT OF DN200

Results show that $10^{11}\ N/m$ is the optimal contact stiffness value that allows obtaining a consistent system response during the contact phase minimizing oscillations and lowering steady-state error. This contact stiffness value allows good flexibility between the contacting bodies, reducing unwanted oscillations or system instability. The same iterative process has been applied to calculate the other contact parameters: $c_m = 10^5\ Ns/m$, $d = 10^3\ m$, $e = 2.2$. The male and female cuffs are made of stainless steel with a surface coating of molybdenum disulfide (MoS_2) to reduce friction and prevent cold welding. The typical static friction coefficient μ_s for the MoS_2 surface coating is $\mu_s = 0.19$ and the coefficient of dynamic friction is $\mu_d = 0.16$ [37].

5.2 Cuffs Geometry

Two different cuffs versions, $v1$ and $v2$, has been proposed for the LBJ, their design are reported in **FIGURE 17**.

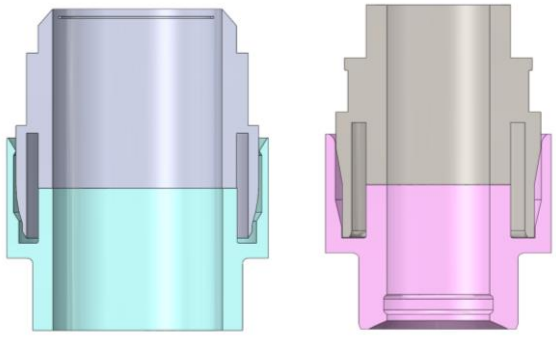

FIGURE 17: CONTACT POINTS BETWEEN CUFFS

In the v2 version, different contact points between female and male cuffs have been designed to enhance alignment during pipe coupling. Both cuff versions have been shaped with alignment features to progressively attain the desired position. The compliance is provided by flexible bellows and constraining rings. The alignment task terminates with contact between bump stops. The results of the primary alignment phase with different cuff designs are presented in the next paragraph.

6. RESULTS AND DISCUSSION

The LBJ multibody model was tested in a simulated environment with two different cuff designs to evaluate the misalignment error and system response by changing cuff shapes, as shown in **FIGURE 18**. An incremental step force without gravity contribution has been used to evaluate cuffs alignment, a $0.1\ m$ starting cuffs surface distance has been imposed.

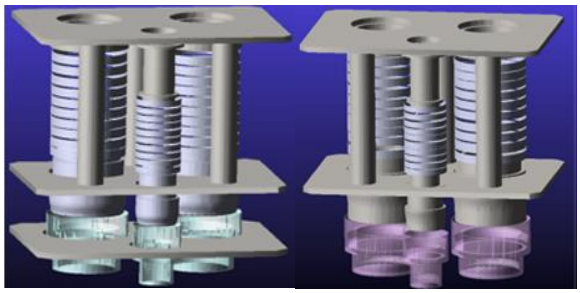

FIGURE 18: MULTIBODY MODELS WITH THE TWO VERSIONS OF CUFFS

Two different cases have been investigated for each cuffs design: cuffs without initial misalignment, and imposing an initial radial misalignment of $2\ mm$ between the cuffs. The results of the simulation are reported below.

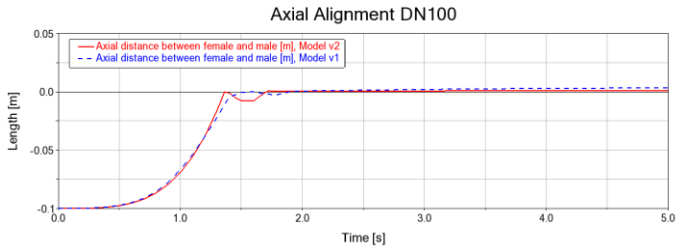

FIGURE 19: AXIAL ALIGNMENT OF DN100

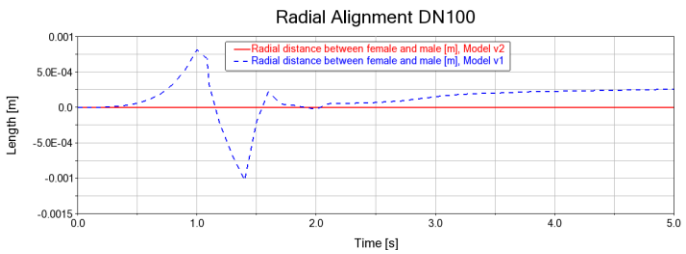

FIGURE 20: RADIAL ALIGNMENT OF DN100

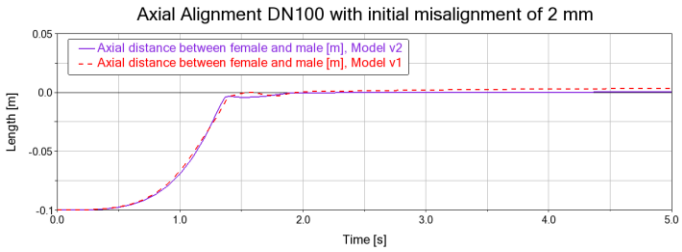

FIGURE 21: AXIAL ALIGNMENT OF DN100 WITH RADIAL MISALIGNMENT

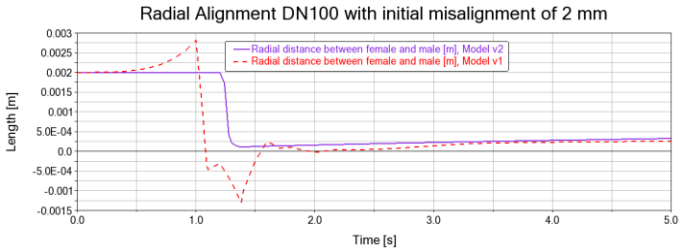

FIGURE 22: RADIAL ALIGNMENT OF DN100 WITH RADIAL MISALIGNMENT

During the simulation, the cuffs model v1 exhibited higher oscillations compared to cuffs v2, with an amplitude two orders of magnitude greater. Furthermore, cuffs v2 guaranteed minor axial distance between surfaces when the alignment phase ends. Results prove the relevance of cuffs design in the alignment phase, the cuffs v2 guarantees minor axial misalignment and minor system vibration.

7. CONCLUSION

This paper presents the high-fidelity model of the Laser Bore Joint (LBJ), focusing on the pipe bundle coupling mechanism. The flexible elements of the LBJ, named bellows, that offer compliance in both axial and radial directions during alignment tasks have been described using both analytical and Finite Element Analysis (FEA). The bellow stress-strain diagram has been obtained, its use allows the determination of the maximum force that induces bellow plasticity. Therefore, a Lumped Parameter Model (LPM) of the bellow has been proposed to reduce load and time computation. Furthermore, the multibody model of the Laser Bore Joint (LBJ) in Adams environment has been presented. Finally, the influence of contact parameters and two different cuff designs on the alignment of the LBJ have been analyzed.

The simulation results evidence the influence of cuff design and contact parameters on the alignment phase. The LPM of the bellow allows the reduction of the computational load while preserving the system dynamics. The proposed alignment procedure could be further refined and applied to other remote maintenance scenarios.

Future works will explore the effects of thermal expansion of the bellows on the alignment accuracy. Additionally, different pipe orientations will be simulated and tested. Finally, experimental validation of the proposed coupling procedure using a test bench will be performed.

ACKNOWLEDGEMENTS

This work has been carried out within the framework of the EUROfusion Consortium, funded by the European Union via the Euratom Research and Training Programme (Grant Agreement No 101052200 — EUROfusion). Views and opinions expressed are however those of the author(s) only and do not necessarily reflect those of the European Union or the European Commission. Neither the European Union nor the European Commission can be held responsible for them.

REFERENCES

[1] Federici, G., et al., “Overview of the DEMO staged design approach in Europe.” Nuclear Fusion, 2019, doi: 10.1088/1741-4326/ab1178.

[2] Federici, G., et al., “Overview of EU DEMO design and R&D activities.” Fusion Engineering and Design, 2014, doi: 10.1016/j.fusengdes.2014.01.070.

[3] Ciattaglia, S., et al., “EU DEMO safety and balance of plant design and operating requirements. Issues and possible solutions.” Fusion Engineering and Design, 2019.

[4] Bachmann, C., et al., “Conceptual study of the remote maintenance of the DEMO breeding blanket.” Fusion Engineering and Design, 2022.

[5] Crofts, O., et al., “Overview of progress on the European DEMO remote maintenance strategy.” Fusion Engineering and Design, 2016,

[6] Hong, S.-H., “A review of DEMO reactor concepts: open questions and issues.” AAPPS Bulletin, 2022, doi: 10.1007/s43673-022-00040-9.

[7] Bolt, H., et al., “Materials for the plasma-facing components of fusion reactors.” Journal of nuclear materials, 2004, doi: 10.1016/j.jnucmat.2004.04.005.

[8] Richiusa, M. L., et al., “Rationale Behind EU-DEMO Limiter’s Plasma-Facing Component Design Under Material Phase Change.” IEEE Transactions on Plasma Science, 2022, doi: 10.1109/TPS.2022.3169232.

[9] Barrett, T. R., et al., “Progress in the engineering design and assessment of the European DEMO first wall and divertor plasma facing components.” Fusion Engineering and Design, vol. 109–111, pp. 917–924, 2016, doi: 10.1016/j.fusengdes.2016.01.052.

[10] Keech, G., et al., “Issues of the vertical blanket segment architecture in DEMO: Current progress and resolution strategies.” Fusion Engineering and Design, vol. 146, 2019, doi: 10.1016/j.fusengdes.2019.02.029.

[11] Keogh, K., et al., “Laser cutting and welding tools for use in-bore on EU-DEMO service pipes.” Fusion Engineering and Design, vol. 136, 2018, doi: 10.1016/j.fusengdes.2018.02.098.
[12] Tremethick, T., et al., “Service Joining Strategy for the EU DEMO.” Fusion Engineering and Design, vol. 158, 2020, doi: 10.1016/j.fusengdes.2020.111724.
[13] Kirk, S., et al., “Remote in-bore laser cutting andwelding tools for use in future nuclear fusion reactors.” Waste Management Symposia, Phoenix, USA, 2018.
[14] Palmieri, P., et al., “Inflatable Robotic Manipulator for Space Debris Mitigation by Visual Servoing.” 2023 9th International Conference on Automation, Robotics and Applications (ICARA). IEEE, 2023. doi: 10.1109/ICARA56516.2023.10125753.
[15] Crofts, O., et al., “EU DEMO Remote Maintenance System development during the Pre-Concept Design Phase.” Fusion Engineering and Design, vol. 179, 2022, doi: 10.1016/j.fusengdes.2022.113121.
[16] Babin, B. R., and Peterson, G. P., “Experimental investigation of a flexible bellows heat pipe for cooling discrete heat sources.” ASME. J. Heat Transfer, vol. 112, no. 3, pp. 602–607, 1990, doi: 10.1115/1.2910429.
[17] Becht IV, C., “Fatigue of bellows, a new design approach.” International journal of pressure vessels and piping, vol. 77, no. 13, pp. 843–850, 2000, doi: 10.1016/S0308-0161(00)00078-8.
[18] Plumridge, J. M., Ketch, D. P., and Straszewski, C. J., “Mechanical seals: the current status of metal bellows sealing.” Tribology international, vol. 19, 1986, doi: 10.1016/0301-679X(86)90056-3.
[19] Day, C. and Giegerich, T., “Development of Advanced Exhaust Pumping Technology for a DT Fusion Power Plant.” IEEE Transactions on Plasma Science, vol. 42, no. 4, 2014, doi: 10.1109/TPS.2014.2307435.
[20] Loving, A., et al., “Pre-conceptual design assessment of DEMO remote maintenance.” Fusion Engineering and Design, vol. 89, no. 9–10, pp. 2246–2250, 2014, doi: 10.1016/j.fusengdes.2014.04.082.
[21] Ando, M., et al., “Experimental demonstration of failure modes on bellows structures subject to internal pressure.” American Society of Mechanical Engineers, 2017, doi: 10.1115/PVP2017-65226.
[22] Abdo, E., Baronio, E., Mauro, S., Troise, M., and Salamina, L., “Case Study of the Use of a Digital Twin for Leak Detection and Quantification in Underground Gas Storage Wells.” SPE Journal, vol. 28, no. 5, pp. 2415–2424, 2023, doi: 10.2118/214357-PA.
[23] Anderson, W. F., “Analysis of Stresses in Bellows, Part I: Design Criteria and Test Results.” NAA-SR-4527. Atomics International Division of North American Aviation, October 15, 1964.
[24] Anderson, W. F., "Analysis of Stresses in Bellows, Part II: Mathematical." NAA-SR-4527 (PT. II), Atomics International Division of North American Aviation, May 27, 1965.
[25] Becht, C., “Predicting bellows response by numerical and theoretical methods.” ASME. J. Pressure Vessel Technol. August 1986; 108(3): 334–341. https://doi.org/10.1115/1.3264794
[26] Troise, M., Gaidano, M., Palmieri, P., and Mauro, S., “Preliminary Analysis of a Lightweight and Deployable Soft Robot for Space Applications.” Applied Science, vol. 11, no. 6, p. 2558, 2021, doi: 10.3390/app11062558.
[27] Palmieri, P., Gaidano, M., Ruggeri, A., Salamina, L., Troise, M., and Mauro, S., “An Inflatable Robotic Assistant for Onboard Applications.” Proceedings of the International Astronautical Congress, IAC. International Astronautical Federation, IAF, 2021.
[28] Troise, M., Sorli, D., Palmieri, P., Gaidano, M., Melchiorre, M., and Mauro, S. “Analysis and Modeling of the Laser Bore Joint To Prevent Alignment Failures.” ASME International Mechanical Engineering Congress and Exposition. American Society of Mechanical Engineers, 2023. doi: 10.1115/IMECE2023-113435.
[29] Arranz, F., et al., "Remote handling in the accelerator systems of DONES." IEEE Transactions on Plasma Science, vol. 48, 2020, doi: 10.1109/TPS.2020.2969262.
[30] Shankar, V., Bhanu Sankara Rao, K., and Mannan, S. L., “Microstructure and mechanical properties of Inconel 625 superalloy,” Journal of nuclear materials, vol. 288, 2001, doi: 10.1016/S0022-3115(00)00723-6.
[31] Expansion Joint Manufacturers Association. Standards of the Expansion Joint Manufacturers Association, 1980.
[32] Salamina, L., Botto, D., Mauro, S., and Pastorelli, S., “Modeling of flexible bodies for the study of control in the simulink environment.” Applied Sciences, vol. 10, no. 17, 2020, doi: 10.3390/app10175861.
[33] Bertolino, A. C., Mauro, S., Jacazio, G., and Sorli, M. Multibody dynamic model of a double nut preloaded ball screw mechanism with lubrication." ASME International Mechanical Engineering Congress and Exposition. Vol. 84553. American Society of Mechanical Engineers, 2020.
[34] Bacci, A., Bertolino, A. C., De Martin, A., and Sorli, M., "Multiphysics modeling of a faulty rod-end and its interaction with a flight control actuator to support phm activities." *ASME International Mechanical Engineering Congress and Exposition*. Vol. 85628. American Society of Mechanical Engineers, 2021.
[35] Bertolino, A. C., De Martin, A., Fasiello, F., Mauro, S., and Sorli, M, "A simulation study on the effect of lubricant ageing on ball screws behaviour." *2022 International Conference on Electrical, Computer, Communications and Mechatronics Engineering (ICECCME)*. IEEE, 2022.
[36] Giesbers, J., “Contact Mechanics in Msc Adams,” p. 42, 2012.
[37] Singer, I. L., et al. “Hertzian stress contribution to low friction behavior of thin MoS 2 coatings,” Applied Physics Letters, vol. 57, no. 10, pp. 995–997, 1990, doi: 10.1063/1.104276.